Chemical Engineering Science 283 (2024) 119369

Contents lists available at ScienceDirect

Chemical Engineering Science

journal homepage: www.elsevier.com/locate/ces

# Enhancement of ozonation using microbubbles – Micropollutant removal, mass transfer and bromate formation

Alexander John [a], Irene Carra [a], Bruce Jefferson [a], Lucie Bertolaso [a], Adam Brookes [b], Peter Jarvis [a,*]

[a] Cranfield University, UK
[b] Anglian Water, Thorpe Wood House, Peterborough, UK

ARTICLE INFO

*Keywords:*
Microbubbles
Pesticides
Ozonation
Drinking water
Mass transfer

ABSTRACT

Microbubble technology is a promising development in the optimisation of gas–liquid contacting processes. When applied to ozonation, microbubbles have demonstrated significant enhancements to mass transfer, dissolved ozone residual and the speed and extent of compound removal. However, the mechanism by which microbubbles enhance performance over conventional bubbles is not well understood and numerous explanations exist within the literature. To elucidate the critical components that drive such enhancements the performance of microbubbles (Sauter mean diameter 37 μm) and conventional bubbles (5.4 mm) were compared under identical conditions in terms volumetric mass transfer coefficient, steady state dissolved ozone concentration, rate constant for ozone self-decomposition and the rate constant for degradation of two pesticides: mecoprop and metaldehyde. Overall, the improvement observed in performance can be attributed to the increase in the volumetric mass transfer coefficient through the combination of an increase in specific interfacial area and a decrease in the mass transfer coefficient. The increase in area outweighed the decrease in mass transfer coefficient such that an overall improvement factor of 1.6 was observed for microbubbles over conventional bubbles. All other differences were an artefact of the enhanced mass transfer leading to higher dissolved ozone concentrations when operating at a fixed input dose. For the first time it has been shown that when normalised to the amount of ozone transferred to the water, no enhancement in hydroxyl radical production, bromate formation or impact from the background constituents could be observed.

## 1. Introduction

Over the past decade, microbubble technology has emerged as a promising route for enhancement of a number of processes that utilise bubbles, including vegetable growth (Tamaki et al., 2020), the ripening and removal of residual pesticides on fruit products (Li et al., 2021; Pongprasert et al., 2020), fisheries aeration (Heriyati et al., 2021), biodiesel production (Ahmad et al., 2019) and in gas–liquid contacting processes for water and wastewater treatment (Marbelia et al., 2020; Thomas et al., 2020; Dong et al., 2023). One commonly applied process where transfer of gas into the liquid phase is required in water treatment is ozonation due to its oxidising and disinfection capabilities (Seridou and Kalogerakis, 2021). Molecular ozone ($O_3$) is an unstable, powerful oxidant with a standard oxidation potential of 2.07 V (Jin et al., 2022). When ozone dissolves in water, it undergoes a series of complex self-decomposition reactions in which numerous short-lived radicals, including the hydroxyl radical, are formed. Hydroxyl radicals are a non-selective, powerful oxidant with a standard oxidation potential of 2.8 V (Wang et al., 2018) which makes the production of hydroxyl radicals desirable. Accordingly, in ozone-based water treatment, the removal of contaminants proceeds through either direct reactions with molecular ozone or through indirect reactions with hydroxyl radicals. Ozonation is particularly useful in the removal of colour (Khuntia et al., 2016), aromatic organic compounds (Nam et al., 2021), pharmaceuticals (Azuma et al., 2019; Paucar et al., 2019), pesticides (Ikehata and El-Din, 2005) and a wide variety of other micropollutants (Derco et al., 2021). Whilst highly effective, the operational cost of ozonation is significant due to its relatively low mass transfer efficiency (Huang et al., 2020; Jodzis and Zięba, 2018), low solubility (Yang et al., 2021), losses through off-gas (Zhang et al., 2018) and its inability to be stored due to its instability (John et al., 2022a).

Ozone is typically delivered through conventional millimetre-sized bubbles. As such, one potential route for enhancing the process is to reduce bubble size to within the range 1–100 μm (microbubbles) using

* Corresponding author.

https://doi.org/10.1016/j.ces.2023.119369
Received 10 May 2023; Received in revised form 13 September 2023; Accepted 5 October 2023
Available online 10 October 2023

recently developed generator technology such as turbulent flow, mechanical shear, pressurised dissolution and forced bubble detachment microbubble generators (John et al, 2022a). Studies using microbubbles have confirmed microbubbles offer: increased interfacial area (Temesgen et al., 2017), lower rise velocity (Swart et al., 2020), enhanced gas utilisation efficiency (Zheng et al., 2015; Muroyama et al., 2013), increased rate of mass transfer (Wu et al., 2019) and increased rate of contaminant removal (Cheng et al., 2019; Lee et al., 2019) when compared with conventional bubbles (Table 1). For instance, the volumetric mass transfer coefficient has been reported to be as much as 5.2 times higher when using microbubbles over conventional bubbles (Zheng et al., 2015). Hu and Xia (2018) reported a steady state dissolved ozone concentration that was 15.8 times higher with microbubble ozonation compared with conventional. Numerous authors have reported enhancements in the removal of a variety of compounds when using microbubbles with enhancement ratios ranging from 1.63 (Khuntia et al., 2016) to 30 (Hu and Xia, 2018). However, the mechanism by which performance is enhanced is not well understood. Several mechanisms have been proposed to suggest that microbubble ozonation enhances hydroxyl radical production through microbubble collapse (Zheng et al., 2015), faster ozone self-decomposition (Zhang et al., 2018), slower ozone self-decomposition (Nam et al., 2021) and increased ozone consumption (Wu et al., 2019). The hypothesis that microbubbles lead to enhanced hydroxyl radical formation was explored previously, which revealed no difference in radical production for microbubbles (37 μm) and conventional bubbles (5.4 mm) when normalising for effective ozone dose and under typical pH used in operational drinking water treatment plants (pH 6–8) (John et al., 2022b). Thus, the contrast in performance between the two bubble types under these conditions is hypothesised to be driven by mass transfer mechanisms. Another aspect of application of ozonation to surface waters for oxidation and disinfection is the potential risk in relation to the formation of bromate from naturally occurring bromide in the water (Li et al., 2018). This particular aspect has not been widely investigated when ozone microbubbles have been used in laboratory and pilot experiments.

The lack of clarity over the mechanisms by which microbubble systems enhance performance limits the opportunity to optimise such systems or provide robust design procedures. Accordingly, the aim of the current work was to understand the controlling mechanism(s) by which microbubbles enhance the performance of ozonation. To achieve this, a set of controlled experiments directly comparing the removal of the pesticides mecoprop and metaldehyde for both microbubble and conventional bubble ozonation were carried out. In order to assess the mechanism by which the performance was enhanced, controlled mass transfer tests were also conducted. Importantly, the comparison considered effective ozone dose to account for differences in reactor geometry and design, a feature that is not routinely considered in most previous work on microbubbles. A variety of parameters, including the volumetric mass transfer coefficient, steady state dissolved ozone concentration and rate of ozone decomposition were assessed for both microbubble and conventional bubble ozonation at three pH representative of typical water treatment operation (pH 6, 7, 8). A secondary objective was to test the hypothesis that the use of microbubbles during ozonation leads to a greater extent of bromate formation in the ozonation of bromide containing waters when compared with conventional bubbles. This was achieved by undertaking direct-comparison experiments with pre-treated surface water.

## 2. Materials and methods

### 2.1. Chemicals

Metaldehyde (Technical grade, Sigma Aldrich) and mecoprop (Analytical grade, Sigma Aldrich) were used as the target compounds. Sulphuric acid ($H_2SO_4$, technical grade, Fisher) and sodium hydroxide (NaOH, technical grade, Fisher) were used for pH adjustment. Potassium iodide (≥98 %, Merck) was used as the ozone quenching agent. N,N-diethyl-1,4-phenylene diamine (DPD) photometric ozone tests (Merck) were used to measure the dissolved ozone concentration. Methanol (Liquid chromatography mass spectrometry (LCMS) grade, ≥ 99.9 %, Fisher) and ultrapure water (18 MΩ, Elga Purelab) were used as the mobile phases for LCMS analysis. Ammonium formate (Technical grade, Sigma Aldrich) was used as the mobile phase buffer for LCMS analysis. Deionized water was obtained from a 15 MΩ, Elga Purelab unit.

### 2.2. Experimental setup

Microbubble and conventional bubble experiments were conducted in a cylindrical acrylic reactor (Model Products) with a height of 80 cm and an inner diameter of 45 cm. When filled with 100 L of liquid, the water height was 62 cm. The experiments were conducted in semi-batch mode (Fig. 1).

Ozone gas was generated from compressed air using a corona discharge ozone generator (C-Lasky C-L010-DT, Advanced Ozone Products) with an operational gas flow rate of 2–10 L $min^{-1}$. For experiments normalised for input ozone gas dose, ozonation was delivered with 100 % output from the ozone generator. The gas flow rate of the

**Table 1**
Mass transfer and kinetics comparison between microbubbles (MB) and conventional bubbles (CB).

| Bubble Diameter | | $k_La/min^{-1}$ | | | $k_D/min^{-1}$ | | | $C_s/mg\ L^{-1}$ | | | $k_a/min^{-1}$ | | | References |
|---|---|---|---|---|---|---|---|---|---|---|---|---|---|---|
| MB/μm | CB/mm | MB | CB | R | MB | CB | R | MB | CB | R | MB | CB | R | |
| <50 | – | 1.38 | 1.15 | 1.2 | – | – | – | 1.2 | 1.11 | 1.08 | – | – | – | Nam et al. (2021) |
| <50 | > 1 | – | – | | – | – | – | 35 | 24 | 1.46 | – | – | – | Sun et al. (2020) |
| 2.35 ± 0.84 | ~ 3 | 0.058 | 0.046 | 1.26 | – | – | – | – | – | – | – | – | – | Gao et al. (2019) |
| 20–50 | mm-size | 0.54 | 0.35 | 1.54 | 0.030 | 0.023 | 1.3 | 2.8 | 2.3 | 1.22 | 0.1 | 0.032 | 3.13 | Wu et al. (2019) |
| 0.25 | mm-size | – | – | – | – | – | – | 10.09 | 0.64 | 15.8 | 0.24 | 0.008 | 30 | Hu and Xia (2018) |
| 51.4 | mm-size | 0.23 | 0.044 | 5.2 | 0.049 | 0.013 | 3.77 | 5.7 | 5.5 | 1.04 | 0.11 | 0.061 | 1.80 | Zhang et al. (2018) |
| – | – | – | – | – | – | – | – | – | – | – | 0.39 | 0.24 | 1.63 | Khuntia et al. (2016) |
| <45 | ~ 1 | 0.34 | 0.23 | 1.48 | – | – | – | 9.6 | 8.4 | 1.14 | – | – | – | Zheng et al. (2015) |
| 15–40 | – | – | – | – | – | – | – | 24 | 9 | 2.67 | 0.099 | 0.032 | 3.09 | Takahashi et al. (2012) |
| 5–50 | 1–5 | 0.095 | 0.109 | 0.87 | – | – | – | 2.5 | 2.2 | 1.14 | 0.0025 | 0.001 | 2.5 | Xu et al. (2012) |
| ~50 | – | 0.32 | 0.25 | 1.28 | – | – | – | – | – | – | – | – | – | Liu et al. (2010) |
| <58 | A few mm | – | – | – | – | – | – | 15 | 14 | 1.07 | 0.16 | 0.091 | 1.76 | Chu et al. (2007) |

$k_La$ is the volumetric mass transfer coefficient ($min^{-1}$).
$k_D$ is the rate constant for ozone self-decomposition ($min^{-1}$).
$C_s$ is the steady state dissolved ozone concentration (mg $L^{-1}$).
$k_a$ is the rate constant for target compound removal ($min^{-1}$).
R is the ratio of microbubble to conventional.

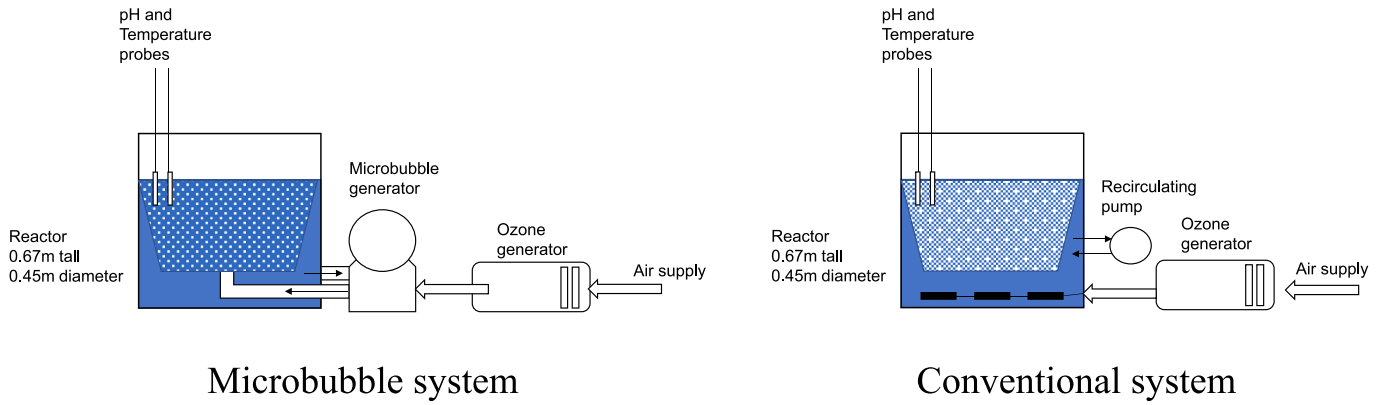


**Fig. 1.** Experimental setup for the microbubble and conventional bubble experiments.

ozone generator was set to 2 L $min^{-1}$, which provided an input (applied) gas phase concentration of 4.75 μmol $L^{-1}$ $min^{-1}$. For the experiments that were normalised for effective ozone dose (equivalent dissolved ozone concentration), the ozone input was manually adjusted until residual ozone concentrations matched for the microbubble and conventional systems. Microbubbles were generated using a regenerative turbine microbubble generator (Nikuni KTM20N trial unit, Aeration & Mixing). The microbubble generator had a recirculating liquid flow rate of 16.6 L $min^{-1}$ and a gas flow meter with a range of 0–5 L $min^{-1}$. The aqueous phase was continuously recirculated through the microbubble generator. Conventional bubbles were generated from a fine pore diffuser (132 mm ceramic air stone diffuser, Finest Aquatic LTD) connected directly to the ozone generator. In order to match the configuration of the microbubble generator as closely as possible, a separate liquid pump (AF-1500, Hidom) with a flow rate of 16.6 L $min^{-1}$ was used to recirculate the aqueous phase for the conventional bubble experiments.

The pH was measured using a portable pH meter (HI-8424, Hanna Instruments), water resistant pH electrode (HI-1230B, Hanna Instruments) and temperature probe (HI-7662, Hanna Instruments). The pH was modified using sodium hydroxide or sulfuric acid. The pH was maintained ± 0.1 throughout each experiment with dropwise addition of dilute sodium hydroxide or sulfuric acid without buffer. The aqueous temperature for all experiments was 20 ± 1 ℃. The starting temperature of the water in all experiments was 20 ± 1 °C and this did not deviate by more than 1 °C during the course of the experiments.

For the single micropollutant removal experiments, an initial concentration of 0.056 μmol/L of metaldehyde or mecoprop was used throughout (equivalent to 10 μg and 12 μg/L respectively). A 20 mL aliquot was removed at pre-defined time intervals and immediately quenched with 200 μL potassium iodide solution to cease ozonation. 10 mL of sample was used for dissolved ozone measurement with the DPD ozone test and measured using a spectrophotometer (Pharo 300, Spectroquant). A portion of the retained sample was filtered through a 0.2 μm syringe filter (Minisart, Sartorius) for LCMS analysis. For the bromate formation tests, water was taken from a water treatment works (WTW) in the East of England which treats water from a reservoir source. The water was taken before secondary ozone and following pre-ozone, coagulation, clarification and rapid gravity filtration treatment. During the experiments, 120 mL of sample was taken at pre-defined time intervals and immediately quenched with 1.2 mL potassium iodide. 10 mL of sample was used for dissolved ozone measurement using the DPD ozone test and measured using the spectrophotometer. 10 mL of sample was filtered through a 0.2 μm syringe filter for LCMS analysis. The remaining 100 mL of sample was stored in labelled sample bottles for bromate analysis using inductively coupled plasma mass spectrometry (ICP-MS) at an accredited external laboratory.

### 2.3. Pesticide analysis

Mecoprop and metaldehyde concentrations were determined using LCMS (ExionLC, Triple Quad 5500+, Sciex). An Acquity C18 ethylene bridged hybrid column (1.7 μm × 2.1 mm × 50 mm) (Waters) maintained at 60 ℃ was used and the sample injection volume was 10 μL. The mobile phase flow rate was 0.45 mL $min^{-1}$. The mobile phase consisted of ultrapure water with 2 mmol/L ammonium formate (A) and methanol with 2 mmol/L ammonium formate (B). For mecoprop, the initial mobile phase ratio was 95:5 A:B. It was ramped linearly to 5:95 A:B over 3 min and held for 30 s before returning to 95:5 A:B for the final 30 s for a total run time of 4 min per sample. For metaldehyde, the initial mobile phase ratio was 95:5 A:B. It was ramped linearly to 5:95 A:B over 2 min and held for 24 s before returning to 95:5 A:B over 6 s and maintained for 90 s for a total run time of 4 min per sample.

### 2.4. Measurement of bubble size distribution and gas hold-up

Microbubble size distribution was measured using focus-beam reflectance measurement (FBRM 600L, Mettler Toledo) continuously over a period of 30 min. A minimum of 30,000 counts were collected and the instrument range was 1–4000 μm.

Conventional bubble size distribution was measured using high speed video (HERO8, GoPro) mounted to a camera tripod (JB01511-BWW, Joby) with a waterproof LED video light (XShot, Suptig) which was submerged into the water. The camera was focussed on a precision ruler with 1 mm spacing (Precision ruler, Dorcrafts) which acted as a size reference. Video was shot at 240 frames per second for 10 min. The video was slowed to 30 frames per second and desaturated using video editing software (GoPro Studio, GoPro). Image frames from the video were extracted using media software (VLC Media Player, VLAN). The image frames were processed manually using image processing software (ImageJ) and the diameter of in-focus bubbles was measured against the size reference. A minimum of 1000 individual in-focus bubbles were measured for each run for a total of 3000 measurements.

The Sauter mean diameter for the microbubble and conventional bubble distributions were calculated as follows (Abbasian-arani et al., 2021):

$$d_{32} = \frac{\sum n_i d_i^3}{\sum n_i d_i^2} \quad (1)$$

where $d_{32}$ is the Sauter mean diameter (m) and $n_i$ is the number of bubbles with diameter $d_i$ (m). Bubble size distributions were measured at pH 7.

Gas holdup was measured as the gas volume ratio in the reactor, determined from the change in water height following the addition of bubbles using:

$$\varepsilon_g = \frac{H_d - H_0}{H_0} \tag{2}$$

where $\varepsilon_g$ is the gas hold-up, $H_d$ is the height of water in the reactor with bubbles, $H_0$ is the height of water in the reactor with no bubbles.

### 2.5. Theory

The overall degradation rate enhancement of a micropollutant when using microbubbles can be expressed as a function of the mass transfer, ozone self-decomposition and kinetic ratios between microbubble and conventional bubble systems:

$$\varepsilon_{r_a} = f(\alpha_{k_{La}}, \beta_{k_D}, \gamma_{k_{a(O_3)}}, \delta_{k_{a(\bullet OH)}}) \tag{3}$$

where $\varepsilon_{r_a}$ is the observed overall degradation rate enhancement, $\alpha_{k_{La}}$ is the improvement due to mass transfer, $\beta_{k_D}$ is the enhancement due to ozone self-decomposition, $\gamma_{k_{a(O_3)}}$ is the improvement due to the reaction kinetics with ozone, $\delta_{k_{a(\bullet OH)}}$ is the enhancement due to the reaction kinetics with hydroxyl radicals. The purpose of this work was to identify the difference between the use of microbubble and conventional bubble ozonation with regards to how the different factors contribute to the overall improvement in removal.

For this purpose, volumetric the mass transfer coefficients ($k_{La}$) must be compared. The $k_{La}$ is comprised of the liquid side mass transfer co-efficient, $k_L$, and the specific gas to liquid interfacial area, $a$. In a pure semi-batch ozonation system (as used in the current study), with ozone as the only compound in ultra-pure water, the mass balance can be described by:

$$\frac{dC}{dt} = k_L a(C^* - C) + k_D C \tag{4}$$

where $k_L a$ is the volumetric mass transfer coefficient ($min^{-1}$), $C^*$ is the steady state equilibrium dissolved ozone concentration (mg $L^{-1}$), $C$ is dissolved ozone concentration (mg $L^{-1}$) and $k_D$ is the first order rate constant for ozone self-decomposition ($min^{-1}$). For microbubbles, a fit to the model suggest that the average behaviour of the dispersed microbubble phase interacts with the average bulk liquid composition in such a way that the liquid phase controls mass transfer. In the present case, where there is a large reservoir of bubbles which recirculate in the reactor, the gas phase will not change significantly, implying further that the liquid phase will control the system and Equation (4) will hold. When mass transfer reaches equilibrium, the mass balance can be described by (Wu et al., 2019):

$$0 = k_L a(C^* - C_s) - k_D C_s \tag{5}$$

where $C_s$ is the steady state dissolved ozone concentration (mg $L^{-1}$).

Through substitution, $k_L a$ can be determined graphically:

$$\frac{dC}{dt} = (k_L a - k_D)(C_s - C) \tag{6}$$

The $k_L a$ can be found through the measurement of the increase in dissolved ozone concentration over time until a steady state was reached. A plot of $\ln(C_s - C)$ against time has the gradient $(k_L a - k_D)$ which allows for $k_L a$ to be calculated provided that $k_D$ is also known. The $k_D$ can be determined experimentally after a steady state has been reached. Once at a steady state, the ozone generator was turned off. The decrease in ozone concentration against time was measured and $k_D$ is found through a plot of $\ln(C) = k_D t$. In the absence of contaminants, it can be assumed that the only reaction route when ozone is dissolved in deionized water is self-decomposition and follows a first order process (Roustan et al., 1996). The $k_L a$ term can be further analysed by separately calculating the interfacial area ($a$) which can be estimated from:

$$a = \frac{6\varepsilon_g}{d_{32}} \tag{7}$$

where $a$ is the interfacial area ($m^{-1}$); $\varepsilon_g$ is the gas hold-up; $d_{32}$ is the Sauter mean diameter, the dimension used in systems with fine bubbles (Wang et al., 2020). The experimental mass transfer coefficient can then be derived:

$$k_L = \frac{k_L a}{a} \tag{8}$$

where $k_L$ is the mass transfer coefficient (m/s).

The Hatta number (Ha) was calculated to determine whether the reaction between ozone and the pollutant pesticide occurred on the bubble surface or in the bulk liquid phase (Blatkiewicz et al., 2023). Where $Ha > 1$, this indicates that the reaction takes place on the bubble surface film and that the bubble will play an important role in controlling the reaction kinetics. Where $Ha < 1$, this implies that the reaction takes place in the bulk liquid and that mass transfer plays the most important role in controlling reaction kinetics. In the present case, the reactant (ozone) concentration reached a steady state and did not change significantly during the reaction, hence the simplified form of the Hatta term was used (Blatkiewicz et al., 2023):

$$Ha = \frac{\sqrt{(D_{W/O3})_T k}}{k_L} \tag{9}$$

where $k$ is the pseudo-first order rate constant of the reaction, $k_L$ is the bubble mass transfer co-efficient and $D_{W/O3}$ is a coefficient of diffusion of ozone in water, $D_{W/O3}$ can be estimated at temperature T from (Johnson and Davis 1996):

$$(D_{W/O3})_T = 1.10 \times 10^{-6} e^{\left(\frac{-1896}{T}\right)} \tag{10}$$

where T is the experimental temperature in degrees Kelvin.

## 3. Results and discussion

### 3.1. Performance of microbubble ozonation in a synthetic matrix

The rate of removal of both mecoprop and metaldehyde increased as pH increased for both the microbubble and conventional bubble ozonation (Fig. 2). In the case of mecoprop, a pesticide known to be degraded by ozonation, the residual concentration was below 5 % of the initial concentration after 15, 10, and 10 min for the microbubble systems compared to 20, 15 and 15 min for the conventional system for pH values of 6, 7 and 8 respectively. Greater differences were observed in the case of metaldehyde, a pesticide known to be recalcitrant to ozone but degradable by hydroxyl radicals. In this case the residual concentration after 45 min was 58 %, 46 % and 5 % of the initial concentration for the microbubble systems at pHs of 6, 7 and 8 respectively. The corresponding values for the conventional system were 75, 66 and 32 % respectively. Overall, the use of the microbubble systems led to higher removal for a given input ozone dose. Increased pH led to higher rates of removal for both of the pesticides due to the increased rates of formation of the non-selective and strongly oxidative hydroxyl radicals under these conditions (John et al., 2022a).

The pseudo-first order rate constant for the removal of mecoprop at pH 6, 7 and 8 was 0.31 ± 0.01, 0.34 ± 0.02 and 0.37 ± 0.04 $min^{-1}$ respectively for the microbubble system and 0.17 ± 0.02, 0.21 ± 0.02 and 0.25 ± 0.02, respectively for the conventional systems. The corresponding improvement factors between microbubbles and conventional bubbles for each pH condition was 1.8, 1.6 and 1.5 times (Fig. 3). Due to its low reactivity with molecular ozone, the pseudo-first order rate constant for the removal of metaldehyde was much lower than that of mecoprop. To illustrate, the values at pH 6, 7 and 8 were 0.012 ± 0.002, 0.017 ± 0.004 and 0.042 ± 0.004 $min^{-1}$ respectively for the

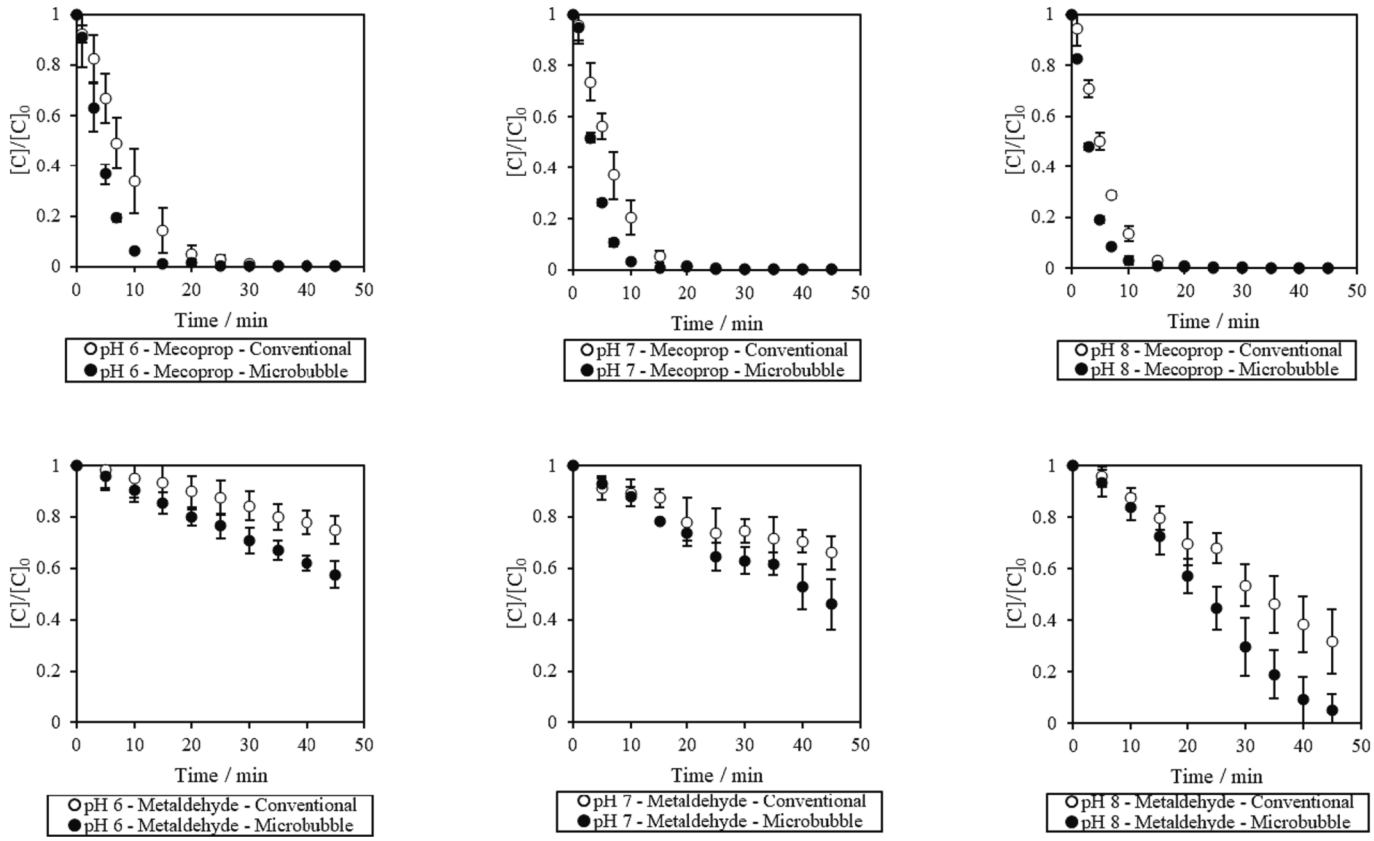


**Fig. 2.** Removal of mecoprop (top) and metaldehyde (bottom) with microbubble and conventional bubble ozonation at pH 6 (left), 7 (middle) and 8 (right).

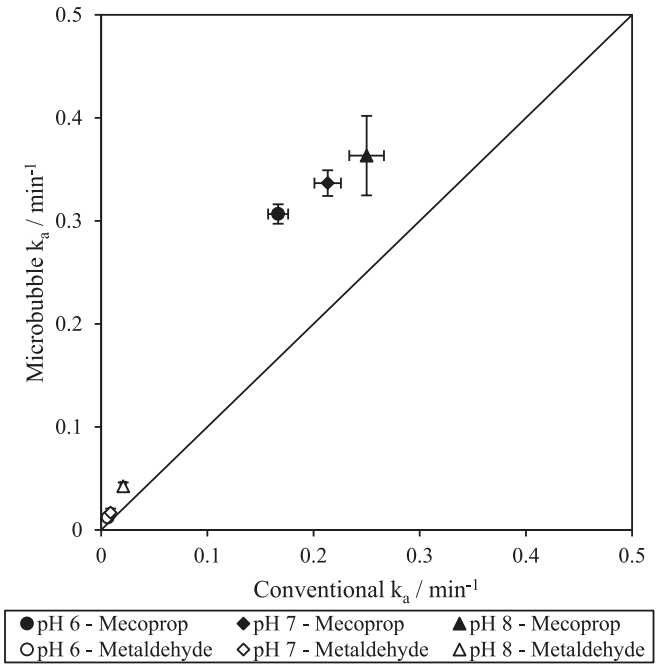


**Fig. 3.** Pseudo first-order rate constants for the removal of metaldehyde and mecoprop for microbubble and conventional bubble ozonation at pH 6, 7, 8.

microbubble system and 0.006 ± 0.001, 0.009 ± 0.002 and 0.021 ± 0.003 $min^{-1}$ for the conventional system. The corresponding improvement factors due to using microbubbles was slightly higher than for mecoprop with values of 2.0, 1.9 and 2.0 times. The current improvement factors are at the low end of those previously reported (Table 1), To illustrate, Wu et al. (2019) observed an average rate constant improvement of 3.4 and 2.8 times for the microbubble ozonation of phenol and nitrobenzene, respectively, across the pH range 3–11. Takahashi et al. (2012) observed a rate constant improvement of 1.1–3.1 times in favour of microbubble ozonation in the removal of four different dyes. All these previous studies use a common input dose and attribute the observed enhancement to increased •OH production (Sun et al., 2020; Wu et al., 2019; Hu and Xia, 2018; Zhang et al., 2018; Wang et al., 2017; Yao et al., 2016; Zheng et al., 2015). Previous research has shown that under the pH conditions used in this study, microbubbles did not produce more hydroxyl radicals than conventional bubbles for a given effective ozone dose (John et al., 2022b). During the final stages of bubble dissolution it has been posited that extremes of pressure and temperature give rise to the formation of hydroxyl radicals during quasi-adiabatic compression (Takahashi et al. 2007; Fan et al., 2023). Given that ozone has relatively low solubility, microbubbles containing this gas may rarely fully dissolve in water, reducing the potential for final bubble dissolution and thus reducing the probability for this mechanism to occur (unlike for more soluble gases such as oxygen). Therefore, the contrast observed in this study between the two bubble systems were related to mass transfer differences, which influenced the effective ozone dose.

To consider this, the data was replotted using the time integral of dissolved ozone concentration (ozone exposure) (Fig. 4). In all cases the comparison of the two systems revealed the same extent and rate of removal for the micropollutants for a given pH, once the standard deviation of experimental replicates was considered. No discernible difference was observed with respect to pH for mecoprop, consistent with its effective reactivity with molecular ozone (Gulde et al., 2021). A clear increase in removal was observed as pH increased for metaldehyde which was consistent with the previously observed increase in •OH production at higher pH for the same experimental system (John et al., 2022b). The •OH driven oxidation is known to be a predominant

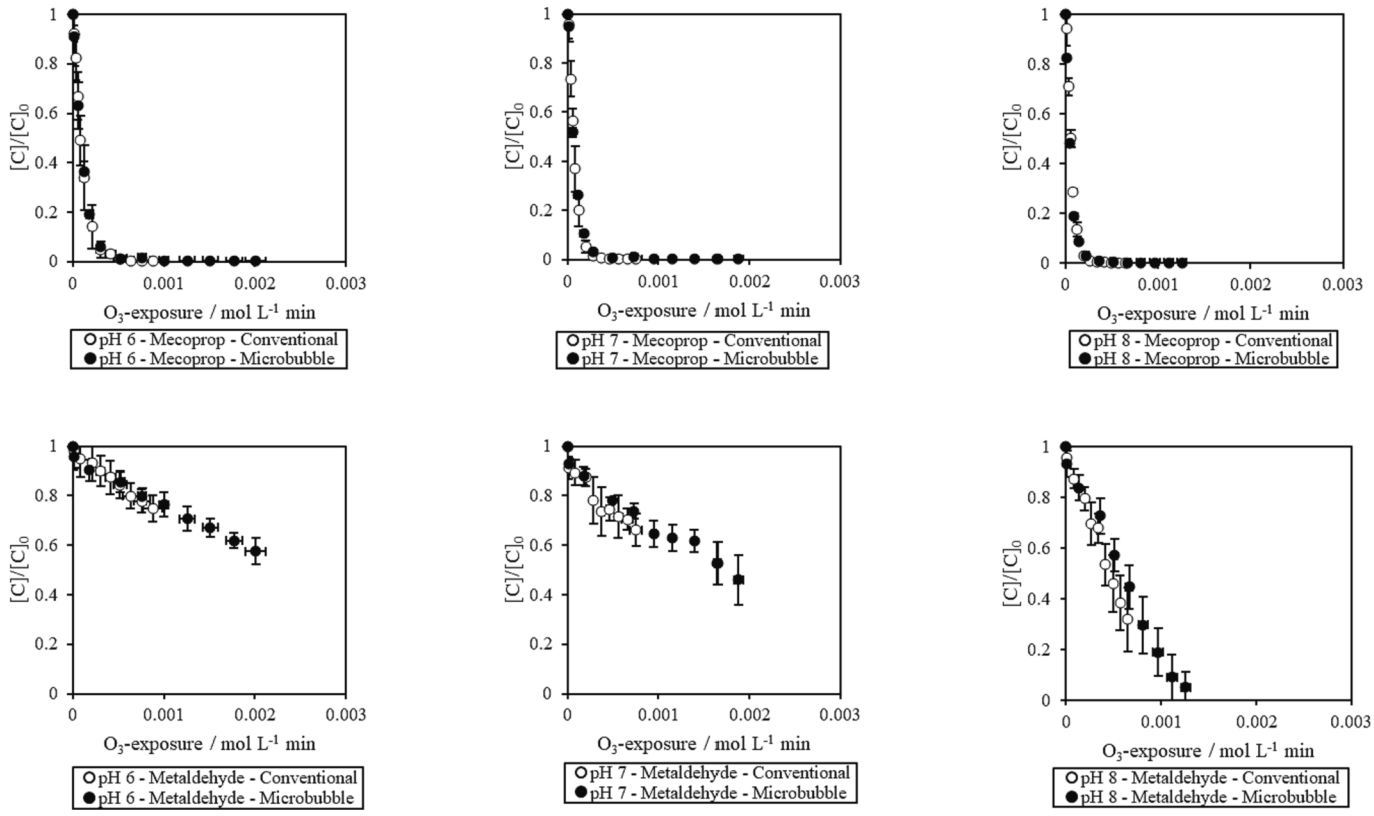


**Fig. 4.** Removal profile of mecoprop (top) and metaldehyde (bottom) normalised against $O_3$-exposure for microbubble and conventional bubble ozonation at pH 6 (left), 7 (middle) and 8 (right).

mechanism of removal for metaldehyde (Tang et al., 2016). Importantly, the conventional bubble system results followed a similar behaviour to the microbubbles, further supporting the view that the smaller microbubbles did not provide an enhanced rate of •OH formation at the higher pH condition (John et al., 2022b). Consequently, the improvements previously reported for MBs are a result of the enhanced mass transfer observed such that the target dissolved ozone dose can be achieved using a reduced input dose. In the current case, this equates to a reduction in input dose of 1.9–2.5 times, identifying potential savings achievable if switching to a microbubble system for ozonation. Regarding the respective mechanisms that are responsible for the observed enhancement, the data above indicates that the $\gamma_{k_{a(O_3)}}$ *and* $\delta_{k_{a(\bullet OH)}}$ terms of Equation (3) (related to the reaction rates between ozone and hydroxyl radicals), are equal to 1 since when normalised for effective dose the degradation rates between the two systems are the same. This implies that microbubbles enhance performance through some function of $k_L$, $a$, $k_La$ and/or $k_D$.

### 3.2. Mass transfer

#### 3.2.1. Steady state concentration and Self-Decomposition

In order to further explore the mechanism by which microbubbles enhance ozonation performance, mass transfer tests were conducted. The increase in dissolved ozone concentration for a fixed input dose was measured over time until a steady state was reached. For conventional bubble ozonation, $C_s$ values of 1.21 ± 0.03, 0.98 ± 0.04 and 0.83 ± 0.03 mg $L^{-1}$ were obtained at pH 6, 7, and 8 respectively (Fig. 5). For microbubble ozonation, the $C_s$ values at pH 6, 7 and 8 were 2.56 ± 0.07, 2.27 ± 0.11 and 1.43 ± 0.04 mg $L^{-1}$. The increase in dissolved ozone at steady state for the microbubble systems represented an enhancement of 2.1, 2.3 and 1.7 times respectively. Previous literature supports the observation of increase in dissolved ozone concentration for a given input dose but with lower ratios that are between 1.1 and 1.7 (Chu et al, 2007; Zheng et al., 2015; Wu et al, 2019). However, differences are to be expected since $C_s$ is influenced by many factors including gas phase ozone input concentration, pH, consumption from reactions with contaminants, gas utilisation efficiency and self-decomposition (Lage Filho,

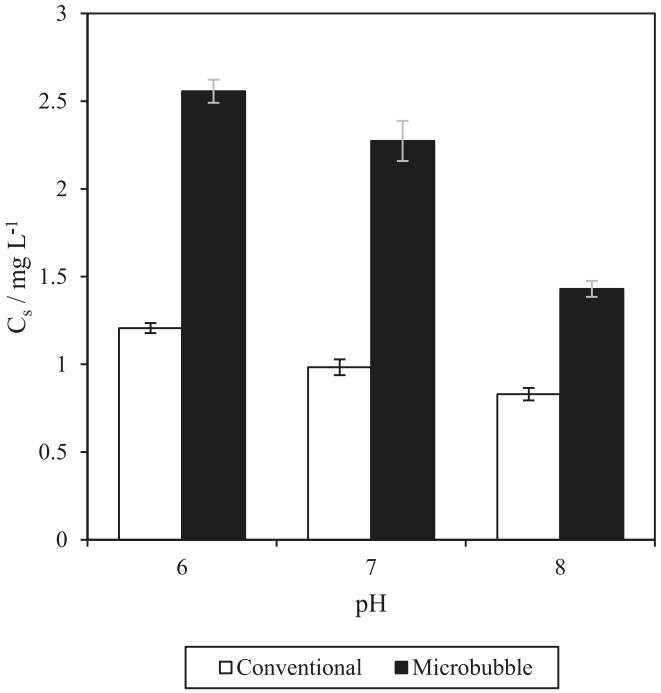


**Fig. 5.** Steady state dissolved ozone concentration for microbubble and conventional bubble ozonation at pH 6, 7, 8.

2010).

Self-decomposition is particularly important due to its link to hydroxyl radical production, involving a complex series of reactions which are pH dependent (Gardoni et al., 2012). To explore this aspect, $k_D$ was determined experimentally by monitoring the decrease in ozone concentration over time (Fig. 6). Self-decomposition rate constants of 0.0016 ± 0.0005, 0.0051 ± 0.0015 and 0.013 ± 0.001 $min^{-1}$ were observed at pHs 6,7 and 8 respectively in the conventional bubble system. These compared to 0.0019 ± 0.0006, 0.0053 ± 0.0012 and 0.013 ± 0.0008 $min^{-1}$ for the microbubble system indicating no discernible difference that could be explained by differences in bubble size. This was confirmed statistically using a Mann-Whitney *U* test with a 95 % confidence interval such that $k_D$ values are the same irrespective of ozone delivery method but vary with pH as expected (Mao et al., 2021). These observations contradict previous reported trials that considered ozone self-decomposition (Wu et al., 2019; Zhang et al., 2018). For instance, Zhang et al. (2018) noted an increase in the rate of ozone self-decomposition from 0.013 $min^{-1}$ to 0.049 $min^{-1}$ when microbubbles were used in place of conventional bubbles; an increase of 3.7 times. However, decreased $k_D$ has also been reported (Nam et al., 2021), where almost no decomposition with microbubbles was observed. In the cases where $k_D$ was increased for microbubbles, this has been proposed to be due to the increased self-decomposition from the production of •OH due to collapsing microbubbles, whilst the justification for observing no decomposition was attributed to the long stagnation time of microbubbles. Evidently, these two observations from the literature infer opposing microbubble behaviour which suggests that some other experimental difference may explain the differences observed in $k_D$. In the current case, no difference in self-decomposition was observed such that the exponent $\beta_{k_D}$ in equation (3) is equal to unity.

### 3.2.2. *Volumetric mass transfer coefficients*

The volumetric mass transfer coefficient ($k_La$) was 0.067 ± 0.009, 0.091 ± 0.005 and 0.15 ± 0.03 for the conventional system and 0.12 ± 0.004, 0.15 ± 0.02 and 0.30 ± 0.03 for the microbubble system as the pH changed from 6 to 7 to 8 respectively (Fig. 7). The corresponding improvement factors (ε) were 1.7, 1.6 and 2.0 due to the use of the microbubble system over that of the conventional bubble system. The improvement factors reported here are at the high end of the range previously reported between 1.2 and 1.8 (Nam et al., 2021; Wu et al., 2019; Zheng et al., 2015; Liu et al., 2010).

The $k_La$ value itself consists of two components: the mass transfer coefficient, $k_L$, and the specific gas-to-liquid interfacial area, *a*. For the microbubbles, there was a relatively narrow distribution with 50 % of the microbubbles having a diameter of < 4.9 μm. The 25th and 75th percentile bubble diameters were 3.1 and 10.0 μm respectively. The Sauter mean diameter, which is the most appropriate diameter model for systems with fine bubbles (Wang et al., 2020), was 37 μm. For the conventional bubbles, the equivalent Sauter mean diameter was 5.4 mm (range 1–10 mm).

The interfacial areas of the microbubble and conventional bubble systems (Equation (7) were 454 and 0.889 $m^{-1}$ for the microbubble and conventional bubble systems respectively, a difference of >510 times. Utilising the values for interfacial area, the experimental values for $k_L$ were calculated as $3.3 \times 10^{-4}$ and $1.0 \times 10^{-1}$ m/s for microbubble and conventional bubble ozonation, respectively at pH 7. The observed increase in $k_L$ for the conventional system compared to microbubble

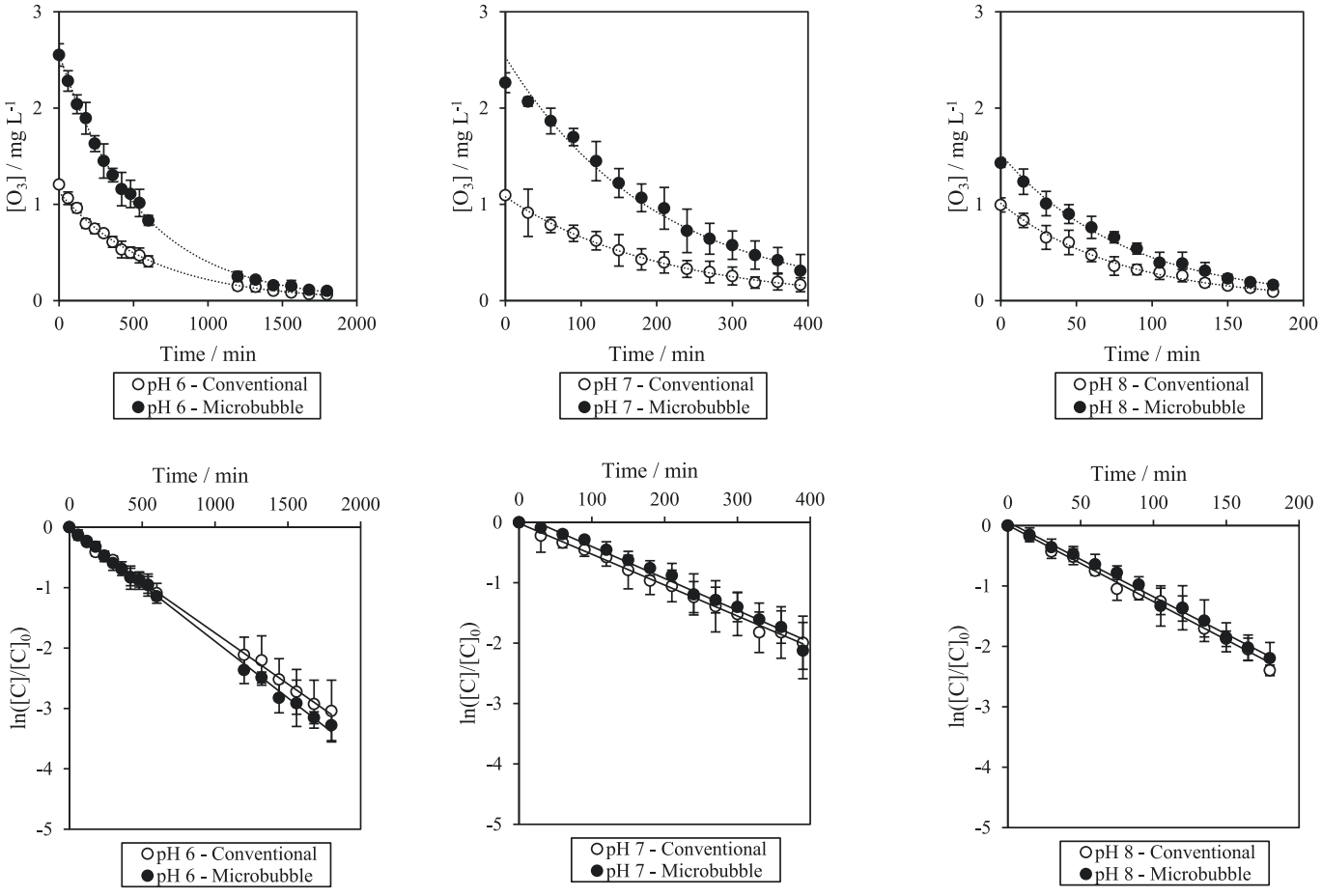


**Fig. 6.** $O_3$ self-decomposition (top) and first order rate constants (bottom) for microbubble and conventional bubble ozonation at pH 6 (left), 7 (middle) and 8 (right).

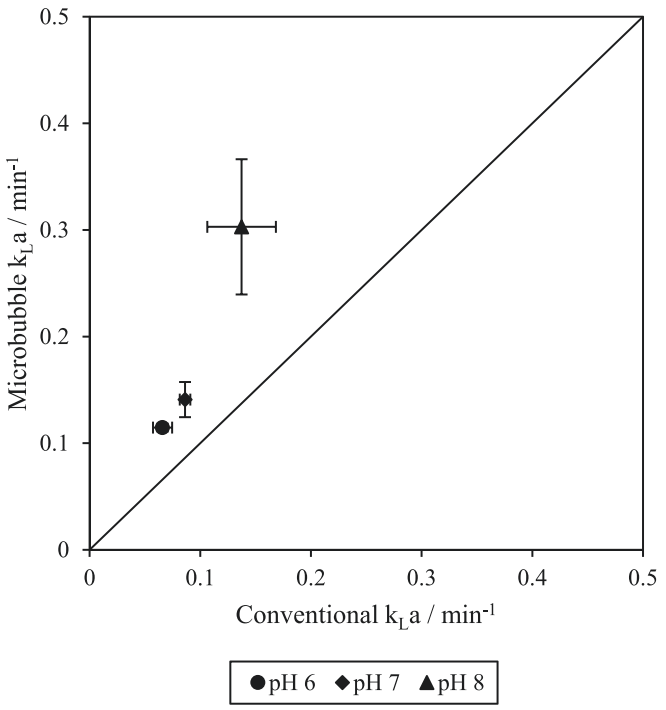


**Fig. 7.** Parity plot of volumetric mass transfer coefficient for microbubble ozonation against conventional bubble ozonation for pH 6, 7, 8.

system is congruent with the work of Kawahara et al, (2009) who noted that $k_L$ increased with an increase in diameter and attributed this to bubble-induced turbulence. This also aligns with the expected reduction in rise velocity observed (relative to that expected of a spherical bubble) for bubbles over 2 mm due to oscillations, deformation of the bubble and increase in drag which slows the bubble and increases residence time allowing more effective dissolution of its contents (Clift et al., 1978).

The improvement factor for microbubble interfacial area was > 500, while the $k_L$ was 303 times less than for the conventional bubbles. This indicates that overall microbubble performance enhancement was a function of the product of the mass transfer coefficient and the interfacial area:

$$\alpha = \theta_{k_L}.\theta_a \tag{11}$$

A comparison of the improvement factors indicates that the overall performance enhancement ($\varepsilon$) was driven by the volumetric mass transfer coefficient ($\alpha_{k_La}$). This in turn was driven by the increase in the mass transfer area ($\theta_a$), which more than compensated for the reduction in the mass transfer coefficient ($\theta_{k_L}$). The implication being that the relationship between overall enhancement and bubble size is a complex balance of the two factors such that an optimum bubble size will likely exist for each system that considers the constituents involved (through the diffusivity) and the hydrodynamics (through the boundary layer thickness).

The Hatta number was calculated to be ≪1 for both bubble systems and for both micropollutants: microbubble – $9.4 \times 10^{-3}$ and $2.0 \times 10^{-3}$; conventional – $2.4 \times 10^{-5}$ and $5.05 \times 10^{-6}$ for mecoprop and metaldehyde respectively under conditions of pH 7. This showed that the reaction kinetics were controlled by the mass transfer of ozone into the bulk water phase for both microbubble and conventional systems. In other words, for both systems, the chemical reaction with the micropollutants was relatively slow compared to the diffusion of ozone into the bulk liquid, hence the reactions occur largely in the bulk liquid rather than the diffusive layer of the conventional and micro sized bubbles.

### 3.3. Influence of microbubble ozonation on micropollutant removal and bromate formation in natural water

In order to determine the performance of the microbubble system for the removal of a micropollutant in a complex matrix and the impact on bromate formation, 0.056 μmol/L of mecoprop was spiked into a part-treated natural water source, representative of a water that would be presented to an ozone process. The background matrix contained 4.1 ± 0.2 mg dissolved organic carbon (DOC) and 100–150 μg/L of bromide. No DOC removal was observed across the ozone exposure experiments. All experiments were performed using water retrieved from the same batch.

The rate constant for the removal of mecoprop in the natural water source using conventional sized bubbles was 0.12 ± 0.01 min$^{-1}$ at pH 6. This value was 70 % of the 0.17 ± 0.02 min$^{-1}$ obtained from the synthetic water experiments (Fig. 8). This compared to 0.22 ± 0.02 min$^{-1}$ in the natural water source and 0.31 ± 0.01 min$^{-1}$ in the synthetic matrix for the microbubble system. The improvement factors in both water matrices were both 1.8, indicating that the presence of other contaminants in the real water did not alter the benefit of using a microbubble system for enhanced mass transfer. The enhanced transfer of more ozone was confirmed from the $O_3$-exposure in the water, which was 1304 ± 75 μmol/L min for the microbubble system and 832 ± 7.5 μmol/L min for the conventional systems, an improvement ratio of 1.6 at pH 6. When the microbubble ozone dose was normalised for effective ozone dose, this resulted in a value close to that seen for the conventional system input dose, with a value of 811 ± 39 μmol/L. A similar observation was seen at pH 7, where the conventional bubble ozone exposure was 651 ± 77 μmol/L min and the microbubble ozone exposure was 711 ± 51 μmol/L min when normalised for effective ozone dose.

Bromate formation is an important operational consideration when

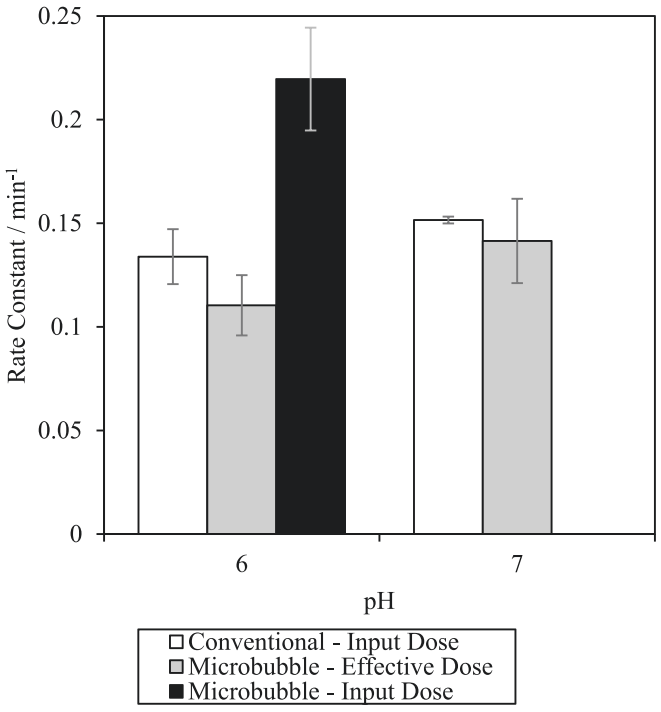


**Fig. 8.** Pseudo-first order rate constants for the removal of mecoprop in part-treated natural water for conventional bubble ozonation (white), microbubble ozonation normalised for effective ozone dose (grey) and microbubble ozonation normalised for input ozone dose (black) at pH 6 and 7 (only two conditions could be assessed due to restrictions in the water volumes that could be collected from the live WTW site - these were chosen based on the closeness to the operational conditions used on site for ozonation).

considering ozone implementation, where it is controlled in drinking water at levels around 0.08 μmol $L^{-1}$ (Jarvis et al., 2007). Here it was shown that the bromate formation followed a linear relationship with ozone exposure that was dependent on pH. The bromate concentrations were 0.054 ± 0.002 μmol/L for conventional bubble ozonation, 0.049 ± 0.001 μmol/L for microbubble ozonation normalised for effective ozone dose and 0.088 ± 0.015 μmol/L for microbubble ozonation normalised for input dose at pH 6. At pH 7, the bromate concentrations were higher, with conventional bubble ozonation resulting in 0.19 ± 0.02 μmol/L, while the bromate concentration for microbubble ozonation normalised for effective ozone dose was 0.21 ± 0.02 μmol/L (Fig. 9). The increased bromate formation at higher pH was expected as a result of the increased formation of $OBr^-$, an important intermediate in the formation of bromate (Song et al., 1996). The results showed that, when normalised for input dose, the total bromate formation was 1.64 times higher for the microbubble system. However, the effective ozone exposure was 1.57 times higher. When normalised for effective ozone dose, there was no significant difference in the extent of bromate formation between the microbubble and conventional bubble systems. Such observations are aligned to the fact that the bromate formation chemistry is dependent on the dissolved ozone concentration. For a fixed effective ozone dose, bromate formation was equivalent in the microbubble and conventional bubble systems. The impact of using microbubble systems is that more ozone transfer is achieved a given input dose. This is primarily due to the increased surface area available for gas diffusion for smaller bubbles, but also due to the increased pressure that results as bubble size decreases (according to the Young-Laplace term). As dictated by Henry's Law, as gas pressure increases, the solubility of the gas in the bubble increases. However, accumulation of compounds on the bubble surface can reduce its surface tension, which in turn will reduce the Laplace pressure in the bubble. Similarly, the role of counter-diffusion of gas into the bubbles remains something of an unknown, particularly in the case of reactive gases such as ozone. Unpicking the influence of each of these factors on gas mass transfer needs to be the focus of future research. The added benefit of the microbubble being that lower ozone input doses would be required to achieve the same effective dose. Further work is required to determine the energy balance of generating microbubbles when compared to conventional bubbles. However, given that there are numerous ways of efficiently generating microbubbles at scale (Zhang et al., 2023), when this is considered alongside the mass transfer benefits observed it is expected that for many applications microbubbles will be a favourable option.

## 4. Conclusion

The work has sought to understand the driving forces behind the reported enhancements that occur when using microbubble systems compared to conventional bubble systems for reactive mass transfer applications such as ozonation in water treatment. Comparison of the different components revealed that the overall enhancement is predominately driven by an improvement in the overall volumetric mass transfer coefficient ($k_La$). For microbubbles, this had two contributions: firstly, a reduction in the mass transfer coefficient ($k_L$) and secondly, an increase in the specific interfacial surface area ($a$). In the case of the microbubble system investigated here, an overall improvement of 1.6 was observed when compared to conventional bubbles, thus the increase in gas transfer area outweighed the reduction in the mass transfer coefficient. No enhancement was observed between microbubbles and conventional bubbles when performance was normalised to a fixed effective ozone dose in terms of ozone self-decomposition or pesticide degradation rate. However, when normalised to input dose all aspects increased and this was related to an increase in the steady state dissolved ozone concentration when microbubbles were applied. The reaction kinetics were shown to be relatively slow compared to the mass transfer

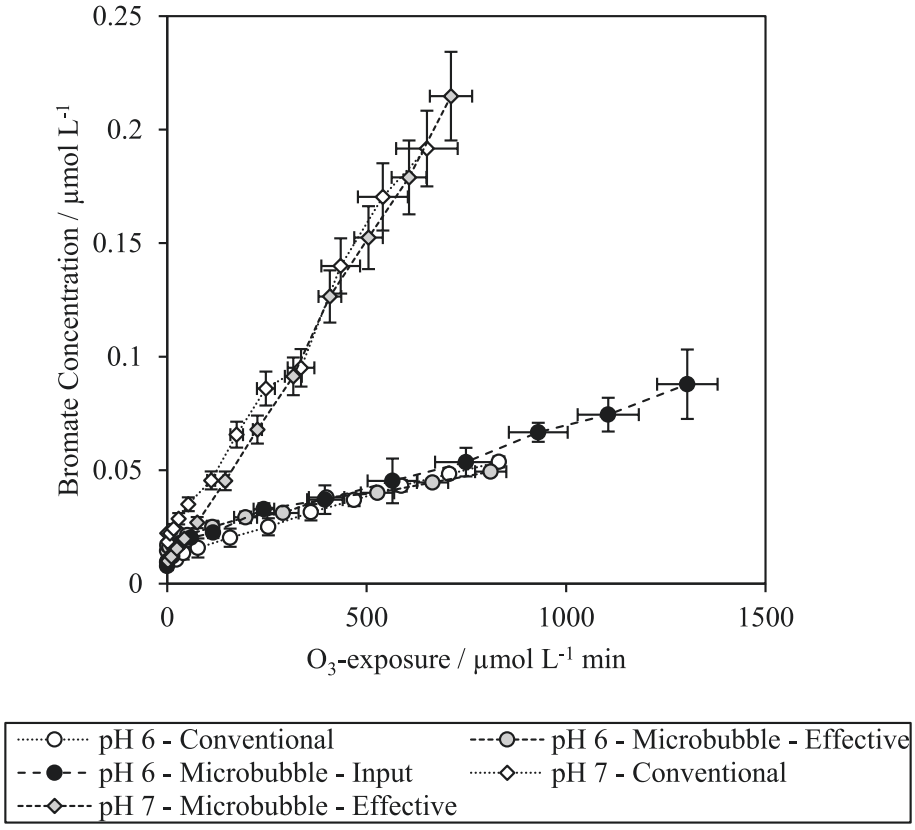


**Fig. 9.** Plot of bromate concentration/μmol/L vs. ozone exposure/μmol/L min in part-treated, pre-ozone natural water for conventional bubble ozonation, microbubble ozonation normalised for effective ozone dose and microbubble ozonation normalised for input ozone dose at pH 6 and 7.

of ozone into the bulk liquid for both microbubble and conventional bubble systems. In the present case, it was therefore demonstrated that the reactions occur largely in the bulk liquid rather than the diffusive layer of the conventional and micro sized bubbles.

Comparison between experiments on synthetic and real waters revealed that the background constituents in the real water did not preferentially impact either the microbubble or conventional bubble systems, resulting in similar improvement factors in both cases. Further, when normalised to effective dose both systems produced the same levels of bromate. The work indicates that future focus should be on understanding the optimum bubble size of any give application based on its impact on both $k_L$ and *a*.

## Declaration of Competing Interest

The authors declare that they have no known competing financial interests or personal relationships that could have appeared to influence the work reported in this paper.

## Acknowledgements

This research is gratefully supported by the Engineering and Physical Sciences Research Council (EPSRC) through their funding of the STREAM Industrial Doctorate Centre (EP/ G037094/1) and from the project sponsor Anglian Water.

## References

Abbasian-arani, M., Hatamipour, M., Rahimi, A., 2021. Experimental determination of gas holdup and volumetric mass transfer coefficient in a jet bubbling reactor. Chin. J. Chem. Eng. 34, 61–67.
Ahmad, N., Javed, F., Awan, J., Ali, S., Fazal, T., Hafeez, A., Aslam, R., Rashid, N., Rehman, M., Zimmerman, W., Rehman, F., 2019. Biodiesel production intensification through microbubble mediated esterification. Fuel 253, 25–31.
Azuma, T., Otomo, K., Kunitou, M., Shimizu, M., Hosomaru, K., Mikata, S., Mino, Y., Hayashi, T., 2019. Removal of pharmaceuticals in water by introduction of ozonated microbubbles. Sep. Purif. Technol. 212, 483–489.
Blatkiewicz, M., Wojtasik-Malinowska, J., Zawadzki, D., Piątkowski, M., Hájek, O., Malý, M., Cejpek, O., Jaskulski, M., 2023. Modeling and simulation of an enzymatic reactive absorption process in the internal zone of a rotating packed bed apparatus. Chem. Eng. Process.-Process Intensif. 189, 109409.
Cheng, W., Jiang, L., Quan, X., Cheng, C., Huang, X., Cheng, Z., Yang, L., 2019. Ozonation process intensification of p-nitrophenol by in situ separation of hydroxyl radical scavengers and microbubbles. Water Sci. Technol. 80 (1), 25–36.
Chu, L., Xing, X., Yu, A., Zhou, Y., Sun, X., Jurcik, B., 2007. Enhanced ozonation of simulated dyestuff wastewater by microbubbles. Chemosphere 68 (10), 1854–1860.
Clift, R., Grace, J.R., Weber, M.E., 1978. Bubbles, Drops, and Particles. Academic Press.
Derco, J., Gotvajn, A., Čižmárová, O., Dudáš, J., Sumegová, L., Šimovičová, K., 2021. Removal of micropollutants by O3-based processes. Processes 9 (6), 1013.
Dong, J., Yao, J., Tao, J., Shi, X., Wei, F., 2023. Degradation of Methyl Orange by ozone microbubble process with packing in the bubble column reactor. Environ. Technol. 44 (17), 2512–2524.
Fan, W., Li, Y., Lyu, T., Chen, Z., Jarvis, P., Huo, Y., Xiao, D., Huo, M., 2023. A modelling approach to explore the optimum bubble size for micro-nanobubble aeration. Water Res. 228.
Gao, Y., Duan, Y., Fan, W., Guo, T., Huo, M., Yang, W., Zhu, S., An, W., 2019. Intensifying ozonation treatment of municipal secondary effluent using a combination of microbubbles and ultraviolet irradiation. Environ. Sci. Pollut. Res. 26 (21), 21915–21924.
Gardoni, D., Vailati, A., Canziani, R., 2012. Decay of O3 in water: A review. $O_3$: Sci. Eng. 34 (4), 233–242.
Gulde, R., Clerc, B., Rutsch, M., Helbing, J., Salhi, E., McArdell, C., von Gunten, U., 2021. Oxidation of 51 micropollutants during drinking water ozonation: Formation of transformation products and their fate during biological post-filtration. Water Res. 207, 117812.
Heriyati, E., Rustadi, R., Isnansetyo, A., Triyatmo, B., Istiqomah, I., 2021. Microbubble aerator test and harvest target prediction based on oxygen consumption of red tilapia (Oreochromis sp.). AACL Bioflux 14 (5), 3006–3022.
Hu, L., Xia, Z., 2018. Application of ozone micro-nano-bubbles to groundwater remediation. J. Hazard. Mater. 342, 446–453.
Huang, X., Quan, X., Cheng, W., Cheng, C., Cheng, Z., Yang, L., Jiang, L., 2020. Enhancement of $O_3$ mass transfer by stainless steel wire mesh and its effect on hydroxyl radical generation. $O_3$: Sci. Eng. 42 (4), 347–356.
Ikehata, K., Gamal El-Din, M., 2005. Aqueous pesticide degradation by ozonation and ozone-based advanced oxidation processes: A review (Part II). Ozone Sci. Eng. 27 (3), 173–202.
Jarvis, P., Smith, R., Parsons, S.A., 2007. Bromate formation during drinking water treatment: an assessment of modelling approaches. Ozone Sci. Eng. 29 (6), 429–442.
Jin, X., Wu, C., Fu, L., Tian, X., Wang, P., Zhou, Y., Zuo, J., 2022. Development, dilemma and potential strategies for the application of nanocatalysts in wastewater catalytic ozonation: A review. J. Environ. Sci. 124, 330–349.
Jodzis, S., Zięba, M., 2018. Energy efficiency of an ozone generation process in oxygen. Analysis of a pulsed DBD system. Vacuum 155, 29–37.
John, A., Brookes, A., Carra, I., Jefferson, B., Jarvis, P., 2022a. Microbubbles and their application to ozonation in water treatment: A critical review exploring their benefit and future application. Crit. Rev. Environ. Sci. Technol. 1–43.
John, A., Carra, I., Jefferson, B., Jodkowska, M., Brookes, A., Jarvis, P., 2022b. Are microbubbles magic or just small? A direct comparison of hydroxyl radical generation between microbubble and conventional bubble ozonation under typical operational conditions. Chem. Eng. J., 134854
Johnson, P.N., Davis, R.A., 1996. Diffusivity of ozone in water. J. Chem. Eng. Data 41 (6), 1485–1487.
Kawahara, A., Sadatomi, M., Matsuyama, F., Matsuura, H., Tominaga, M., Noguchi, M., 2009. Prediction of micro-bubble dissolution characteristics in water and seawater. Exp. Therm Fluid Sci. 33 (5), 883–894.
Khuntia, S., Majumder, S., Ghosh, P., 2016. Catalytic ozonation of dye in a microbubble system: Hydroxyl radical contribution and effect of salt. J. Environ. Chem. Eng. 4 (2), 2250–2258.
Lage Filho, F., 2010. O3 application in water sources: effects of operational parameters and water quality variables on O3 residual profiles and decay rates. Braz. J. Chem. Eng. 27 (4), 545–554.
Lee, Y., Park, Y., Lee, G., Kim, Y., Chon, K., 2019. Enhanced degradation of pharmaceutical compounds by a microbubble ozonation process: effects of temperature, pH, and humic acids. Energies 12 (22), 4373.
Li, P., Wu, C., Yang, Y., Wang, Y., Yu, S., Xia, S., Chu, W., 2018. Effects of microbubble ozonation on the formation of disinfection by-products in bromide-containing water from Tai Lake. Sep. Purif. Technol. 193, 408–414.
Li, C., Xie, Y., Guo, Y., Cheng, Y., Yu, H., Qian, H., Yao, W., 2021. Effects of O3-microbubble treatment on the removal of residual pesticides and the adsorption mechanism of pesticides onto the apple matrix. Food Control 120, 107548.
Liu, S., Wang, Q., Zhai, X., Huang, Q., Huang, P., 2010. Improved pretreatment (coagulation-floatation and ozonation) of younger landfill leachate by microbubbles. Water Environ. Res 82 (7), 657–665.
Mao, Y., Qi, S., Guo, X., Yang, H., Xie, Y., 2021. Optimization of O3 dosage in an O3 contact tank using a numerical model. Environ. Sci. Pollut. Res. 28 (33), 44987–44997.
Marbelia, L., Wan Noor, A., Paramesti, A., Damarjati, B., Widyaparaga, A., Deendarlianto, Bilad, M., Budhijanto, W., 2020. A comparative study of conventional aerator and microbubble generator in aerobic reactors for wastewater treatment. IOP Conf. Series: Mater. Sci. Eng. 778 (1), 012132.
Muroyama, K., Imai, K., Oka, Y., Hayashi, J., 2013. Mass transfer properties in a bubble column associated with micro-bubble dispersions. Chem. Eng. Sci. 100, 464–473.
Nam, G., Mohamed, M., Jung, J., 2021. Enhanced degradation of benzo[a]pyrene and toxicity reduction by microbubble ozonation. Environ. Technol. 42 (12), 1853–1860.
Paucar, N., Kim, I., Tanaka, H., Sato, C., 2019. O3 treatment process for the removal of pharmaceuticals and personal care products in wastewater. $O_3$: Sci. Eng. 41 (1), 3–16.
Pongprasert, N., Srilaong, V., Sugaya, S., 2020. An alternative technique using ethylene micro-bubble technology to accelerate the ripening of banana fruit. Sci. Hortic. 272, 109566.
Roustan, M., Wang, R., Wolbert, D., 1996. Modeling hydrodynamics and mass transfer parameters in a continuous O3 bubble column. $O_3$: Sci. Eng. 18 (2), 99–115.
Seridou, P., Kalogerakis, N., 2021. Disinfection applications of O3 micro- and nanobubbles. Environ. Sci. Nano 8 (12), 3493–3510.
Song, R., Minear, R., Westerhoff, P., Amy, G., 1996. Bromate formation and control during water ozonation. Environ. Technol. 17 (8), 861–868.
Sun, Z., Chen, X., Yang, K., Zhu, N., Lou, Z., 2020. The progressive steps for TPH stripping and the decomposition of oil refinery sludge using microbubble ozonation. Sci. Total Environ. 712, 135631.
Swart, B., Zhao, Y., Khaku, M., Che, E., Maltby, R., Chew, Y., Wenk, J., 2020. In situ characterisation of size distribution and rise velocity of microbubbles by high-speed photography. Chem. Eng. Sci. 225, 115836.
Takahashi, M., Chiba, K., Li, P., 2007. Free-radical generation from collapsing microbubbles in the absence of a dynamic stimulus. J. Phys. Chem. B 111 (6), 1343–1347.
Takahashi, N., Ichikawa, H., Torii, H., Shibata, S., Duy, N., Phuong, P., 2012. Ozonation of dyestuff solutions using a fine bubble generator system. $O_3$: Science and Engineering 34 (3), 196–203.
Tamaki, M., Ikeura, H., Enmei, N., 2020. Growth response of hydroponic leaf lettuce and komatsuna to O3 microbubble treatment. J. Plant Nutr. 43 (10), 1369–1377.
Tang, L.L., DeNardo, M.A., Gayathri, C., Gil, R.R., Kanda, R., Collins, T.J., 2016. TAML/H2O2 oxidative degradation of metaldehyde: pursuing better water treatment for the most persistent pollutants. Environ. Sci. Tech. 50 (10), 5261–5268.
Temesgen, T., Bui, T., Han, M., Kim, T., Park, H., 2017. Micro and nanobubble technologies as a new horizon for water-treatment techniques: A review. Adv. Colloid Interface Sci. 246, 40–51.
Thomas, B., Ohde, D., Matthes, S., Engelmann, C., Bubenheim, P., Terasaka, K., Schlüter, M., Liese, A., 2020. Comparative investigation of fine bubble and macrobubble aeration on gas utility and biotransformation productivity. Biotechnol. Bioeng. 118 (1), 130–141.

Wang, W., Fan, W., Huo, M., Zhao, H., Lu, Y., 2018. Hydroxyl radical generation and contaminant removal from water by the collapse of microbubbles under different hydrochemical conditions. Water Air Soil Pollut. 229 (3).
Wang, H., Wang, Y., Lou, Z., Zhu, N., Yuan, H., 2017. The degradation processes of refractory substances in nanofiltration concentrated leachate using micro-ozonation. Waste Manag. 69, 274–280.
Wang, B., Yang, G., Tian, H., Li, X., Yang, G., Shi, Y., Zhou, Z., Zhang, F., Zhang, Z., 2020. A new model of bubble Sauter mean diameter in fine bubble-dominated columns. Chem. Eng. J. 393, 124673.
Wu, C., Li, P., Xia, S., Wang, S., Wang, Y., Hu, J., Liu, Z., Yu, S., 2019. The role of interface in microbubble ozonation of aromatic compounds. Chemosphere 220, 1067–1074.
Xu, Z., Mochida, K., Naito, T., Yasuda, K., 2012. Effects of operational conditions on 1,4-dioxane degradation by combined use of ultrasound and ozone microbubbles. Jpn. J. Appl. Phys. 51, p. 07GD08.
Yang, X., Liu, Z., Manhaeghe, D., Yang, Y., Hogie, J., Demeestere, K., Van Hulle, S., 2021. Intensified ozonation in packed bubble columns for water treatment: Focus on mass transfer and humic acids removal. Chemosphere 283, 131217.
Yao, K., Chi, Y., Wang, F., Yan, J., Ni, M., Cen, K., 2016. The effect of microbubbles on gas-liquid mass transfer coefficient and degradation rate of COD in wastewater treatment. Water Sci. Technol. 73 (8), 1969–1977.
Zhang, J., Huang, G., Liu, C., Zhang, R., Chen, X., Zhang, L., 2018. Synergistic effect of microbubbles and activated carbon on the ozonation treatment of synthetic dyeing wastewater. Sep. Purif. Technol. 201, 10–18.
Zhang, Z.H., Wang, S., Cheng, L., Ma, H., Gao, X., Brennan, C.S., Yan, J.K., 2023. Micro-nano-bubble technology and its applications in food industry: A critical review. Food Rev. Intl. 39 (7), 4213–4235.
Zheng, T., Wang, Q., Zhang, T., Shi, Z., Tian, Y., Shi, S., Smale, N., Wang, J., 2015. Microbubble enhanced ozonation process for advanced treatment of wastewater produced in acrylic fiber manufacturing industry. J. Hazard. Mater. 287, 412–420.

# Enhancement of ozonation using microbubbles – Micropollutant removal, mass transfer and bromate formation

John, Alexander

2023-10-13



John A, Carra I, Jefferson B, et al., (2024) Enhancement of ozonation using microbubbles – Micropollutant removal, mass transfer and bromate formation. Chemical Engineering Science, Volume 283, January 2023, Article number 119369

https://doi.org/10.1016/j.ces.2023.119369